



Raman spectroscopy links differentiating osteoblast matrix signatures to pro-angiogenic potential



Aikta Sharma^a, Alice Goring^a, Katherine A. Staines^b, Roger J.H. Emery^c, Andrew A. Pitsillides^d, Richard O.C. Oreffo^e, Sumeet Mahajan^f and Claire E. Clarkin^a

a - *School of Biological Sciences, Highfield Campus, University of Southampton, Southampton, SO17 1BJ, United Kingdom of Great Britain and Northern Ireland*

b - *School of Applied Sciences, Sighthill Campus, Edinburgh Napier University, Edinburgh, EH11 4BN, United Kingdom of Great Britain and Northern Ireland*

c - *Department of Surgery and Cancer, Faculty of Medicine, St Mary's Campus, Imperial College London, London, W2 1PG, United Kingdom of Great Britain and Northern Ireland*

d - *Department of Comparative Biomedical Sciences, Royal Veterinary College, London, NW1 0TU, United Kingdom of Great Britain and Northern Ireland*

e - *Centre for Human Development, Stem Cell and Regeneration, Institute of Developmental Sciences, Faculty of Medicine, University of Southampton, Southampton General Hospital, Southampton, SO16 6YD, United Kingdom of Great Britain and Northern Ireland*

f - *School of Chemistry and Institute for Life Sciences, Highfield Campus, University of Southampton, Southampton, SO17 1BJ, United Kingdom of Great Britain and Northern Ireland*

Correspondence to Sumeet Mahajan and Claire E. Clarkin: S.Mahajan@soton.ac.uk, C.E.Clarkin@soton.ac.uk.
<https://doi.org/10.1016/j.mbplus.2019.100018>

Abstract

Mineralization of bone is achieved by the sequential maturation of the immature amorphous calcium phase to mature hydroxyapatite (HA) and is central in the process of bone development and repair. To study normal and dysregulated mineralization in vitro, substrates are often coated with poly-L-lysine (PLL) which facilitates cell attachment. This study has used Raman spectroscopy to investigate the effect of PLL coating on osteoblast (OB) matrix composition during differentiation, with a focus on collagen specific proline and hydroxyproline and precursors of HA. Deconvolution analysis of murine derived long bone OB Raman spectra revealed collagen species were 4.01-fold higher in OBs grown on PLL. Further, an increase of 1.91-fold in immature mineral species (amorphous calcium phosphate) was coupled with a 9.32-fold reduction in mature mineral species (carbonated apatite) on PLL versus controls. These unique low mineral signatures identified in OBs were linked with reduced alkaline phosphatase enzymatic activity, reduced Alizarin Red staining and altered osteogenic gene expression. The promotion of immature mineral species and restriction of mature mineral species of OB grown on PLL were linked to increased cell viability and pro-angiogenic vascular endothelial growth factor (VEGF) production. These results demonstrate the utility of Raman spectroscopy to link distinct matrix signatures with OB maturation and VEGF release. Importantly, Raman spectroscopy could provide a label-free approach to clinically assess the angiogenic potential of bone during fracture repair or degenerative bone loss.

© 2019 Published by Elsevier B.V. This is an open access article under the CC BY-NC-ND license (<http://creativecommons.org/licenses/by-nc-nd/4.0/>).

Introduction

The physiological process of mineralization, central to skeletal development and remodelling, is

regulated by the interactions of minerals with organic extracellular molecules. Today, researchers continue to investigate the vital processes by which mineralized tissues form and repair since suboptimal

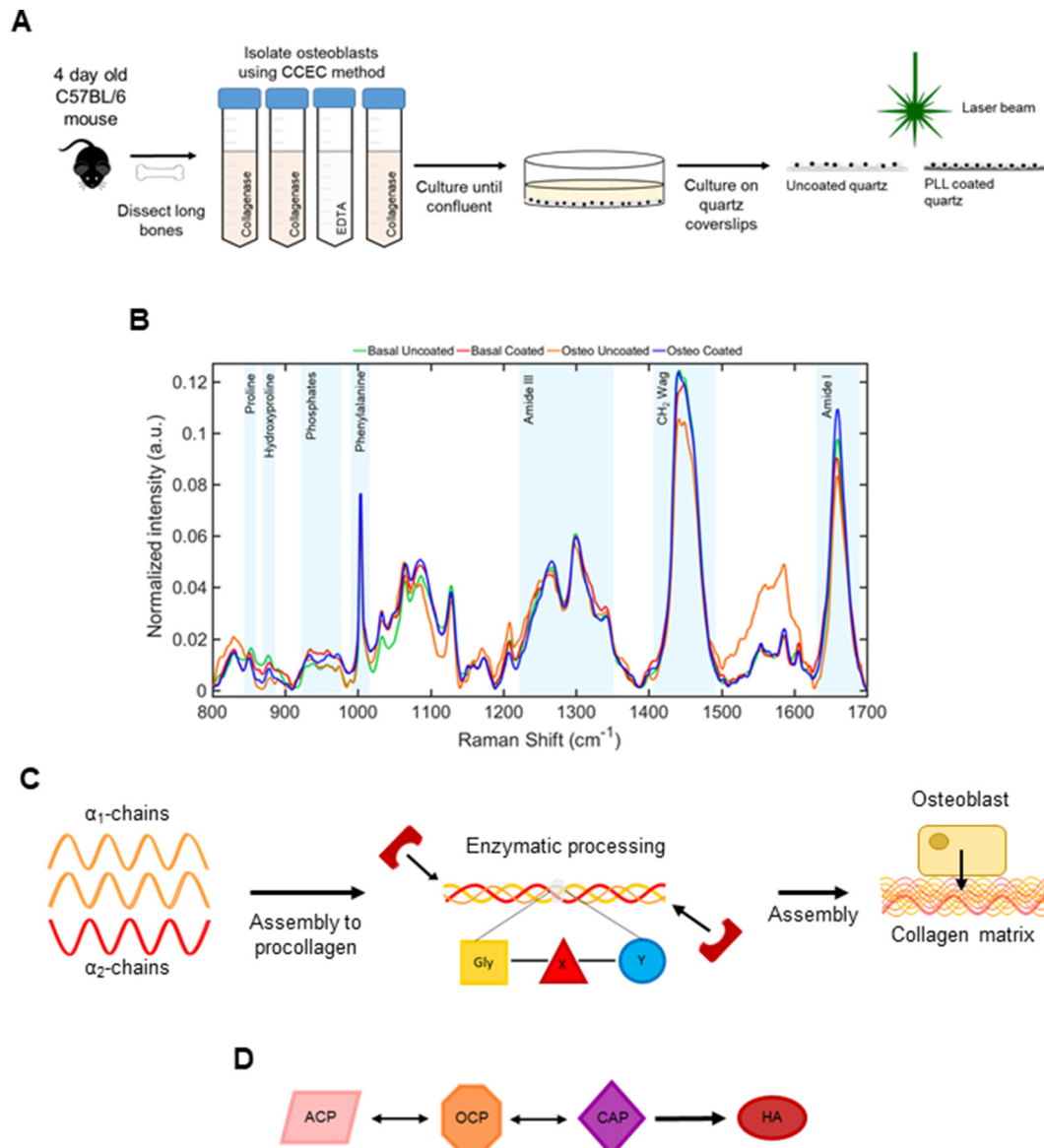


Fig. 1. Raman spectroscopy of primary murine long bone osteoblasts (OBs). OBs were extracted from the long bones of P4 C57BL/6 mice using the collagenase-collagenase-EDTA-collagenase (CCEC) method, then plated onto uncoated or poly-L-lysine (PLL) coated quartz coverslips in basal or osteogenic (osteo) conditions ahead of fixation and Raman spectroscopy (A). Deviations in normalized mean spectral intensity ($n = 125$ spectra; B) were evident in proline (853 cm^{-1}), hydroxyproline (876 cm^{-1}), phosphate region (940 cm^{-1} to 980 cm^{-1}), amide III region (1242 cm^{-1}), CH_2 deformation (1450 cm^{-1}) and amide I (1660 cm^{-1}). Illustration of collagen matrix development from enzymatically processed tropocollagen molecules, α_1 and α_2 -chains (C). Schematic of conversion of mineral species from amorphous calcium phosphate (ACP) to octacalcium phosphate (OCP) and carbonated apatite (CAP) before establishment of mature crystalline hydroxyapatite (HA; D).

or excessive mineralization will directly impact bone structure, mechanical competence and fragility. However, experimental approaches to define the contributions of specific matrix components underlying mineral formation remain limited.

Historically, extracellular matrix (ECM) mineralization in the skeleton was considered a passive process. However, murine studies have identified

mineralization to be temporally regulated and tightly coordinated due to the involvement of multiple genetic pathways [1–8]. Underlying genetic regulation can control; the homeostasis of ionic calcium and inorganic phosphates required for bone mineral formation, synthesis of mineral scaffolding ECM, and maintenance of the inhibitory organic and inorganic mediator levels that control further mineral crystal

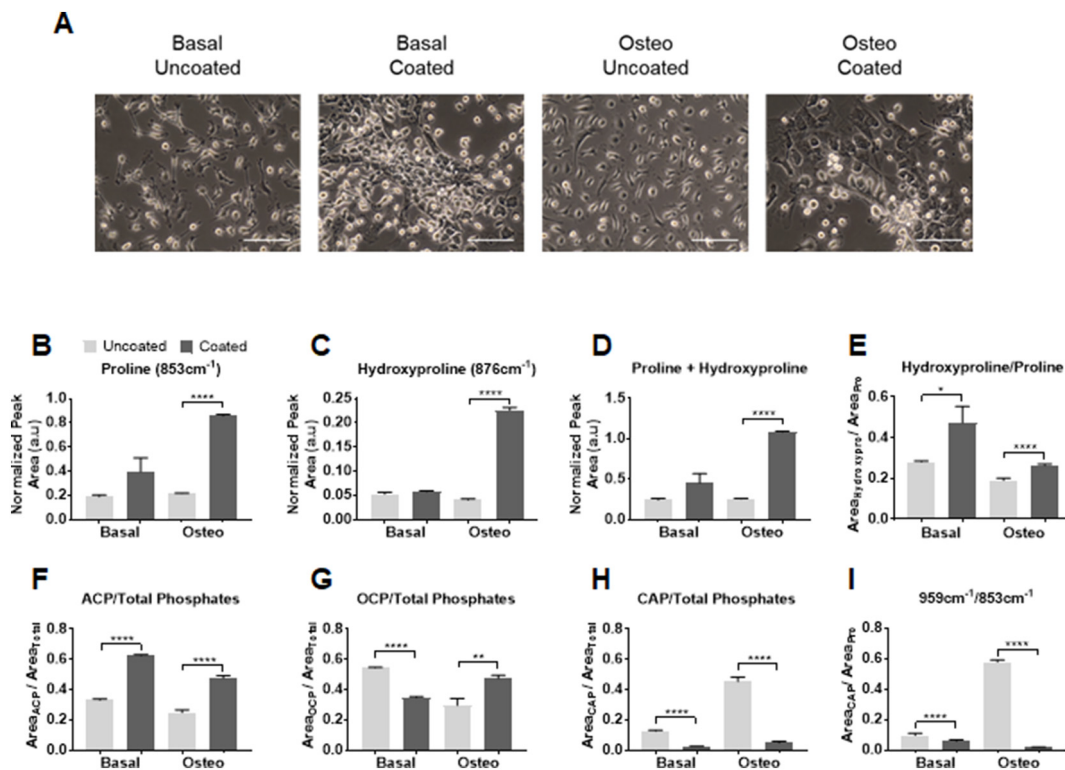


Fig. 2. Promotion of immature mineral and matrix OB signatures on PLL. Representative phase contrast images of OBs (scale bars represent 100 μm) show differences in cell morphology on uncoated versus PLL coated quartz between the basal and osteogenic (osteo) conditions (A). Spectral deconvolution of Raman spectra revealed differences in components of mature collagen (proline; B, hydroxyproline; C and their sum; D) between cultures on uncoated and PLL coated quartz. Collagen intra-strand stability (E), described by the ratio of hydroxyproline to proline, was increased in OB cultures on PLL coated quartz. Fluctuations in immature (ACP; F), intermediate (OCP; G) and mature (CAP; H) mineral species are also detected on PLL coated quartz and are reflected in the mineral/matrix ratio (I). Data presented as the mean normalized peak area \pm standard error of the mean (SEM) from three separate experiments. Statistical significance between conditions was assessed using Student's *t*-test ($P < .05^*$, $P < .01^{**}$, $P < .0001^{****}$).

nucleation. Prior to the formation of the stable form of hydroxyapatite (HA), a range of calcium phosphate intermediates are generated, consisting of amorphous calcium phosphate (ACP), the first insoluble phase of calcium phosphate, followed by transient intermediate forms, octacalcium phosphate (OCP) and subsequently carbonated apatite (CAP) [9,10]. HA crystals have been shown to form inside matrix vesicles (MV) which bud from the surface membrane of hypertrophic chondrocytes and osteoblasts (OBs) [11–14]. It is believed that the combination of inorganic calcium and phosphate ions accumulating inside MVs instigate the breakdown of the MV membrane, releasing HA crystals into the extracellular fluid, to facilitate crystal propagation in and around the collagenous ECM. Locally, in the OB and its microenvironment, phosphatases such as PHOSPHO1 and tissue-nonspecific alkaline phosphatase (ALP) are thought to be key factors in the initiation of mineralization [3]. In tandem, both are functionally responsible for providing phosphates necessary for crystal nucleation and growth within MVs and the

dephosphorylation of local inhibitory pyrophosphate [15,16].

In vitro, the elucidation of the mechanisms which underlie these distinct stages of matrix mineralization is difficult, therefore identifying novel therapeutic candidates which drive deficient or pathological mineralization remains a significant challenge. Molecular approaches to quantify gene expression levels (e.g. *Phospho1*, *Alpl*) are typically used to assess OB differentiation status in vitro and are commonly combined with histological matrix stains including Von Kossa, Alizarin Red or Sirius Red. However, these approaches require considerable sample preparation, are semi-quantitative and, crucially, fail to provide sufficient information to define a specific mineralization stage of individual cells within a population. Raman spectroscopy is an optical, label-free, non-destructive vibrational fingerprinting technique that has been used to detect biochemical changes in a variety of cell types [16–19] in both qualitative and quantitative capacities [20–24]. We have recently used Raman

spectroscopy for the detection of early osteogenic lineage commitment where this approach provided enriched quantitative information regarding the composition of OB ECM in comparison to standard cell differentiation and gene expression assays [25]. Herein, we have used Raman spectroscopy and the effect of poly-L-lysine (PLL) coatings to assess whether distinct mineral and matrix signatures produced by individual OBs are linked to their differentiation status. Furthermore, given that mineralization is driven by the vascular supply to bone we have investigated whether composition of specific mineral and matrix components within the OB ECM influences vascular endothelial growth factor (VEGF) production.

Results

Raman spectroscopy reveals immature mineral and matrix osteoblast signatures on PLL coatings

To study the effect of PLL coating on OB differentiation using Raman spectroscopy, primary murine long bone OBs were isolated from the tibia, fibula and femur of 4-day old (P4) C57BL/6 mice using the CCEC method (Fig. 1A). Cells were cultured under basal or differentiation-promoting osteogenic (osteo) conditions on uncoated or PLL coated quartz coverslips for 19 days before fixation ahead of Raman spectroscopy (Fig. 1A). Previously we have shown that Raman spectroscopy can successfully detect changes in differentiating primary OB cell cultures [25]. Here, we used Raman spectroscopy to quantify changes specifically occurring within the mineral and matrix components of the secreted ECM on these substrates. Specifically, collagen associated matrix bands namely proline and hydroxyproline (853 cm^{-1} and 876 cm^{-1} respectively), CH_2 deformation (1450 cm^{-1}) and amide I (1660 cm^{-1}) in addition to those associated with mineral species in the phosphate region between 940 cm^{-1} and 980 cm^{-1} were also examined (Fig. 1B). During ECM deposition and subsequent mineralization, type I collagen is first processed and secreted by OBs (Fig. 1C) before it is assembled and mineralized through the release of extracellular mineral crystals (Fig. 1D) [13,26,27].

Phenotypic changes in OB morphology were observed between those grown on PLL (Fig. 2A) with cells appearing flatter, closer together with less processes evident versus uncoated controls. Upon the examination of the collagen specific vibrations of proline and hydroxyproline (Fig. 2B and C respectively), small increases were observed in OB cultures on PLL coatings in basal medium compared to uncoated controls (+2.08 and +1.09-fold respec-

tively), which were significantly increased under culture in osteogenic conditions (+4.01 and +5.57-fold respectively). As both proline and hydroxyproline are often considered together, due to their prevalence in the X and Y position of the glycine-X-Y repeat of type I collagen (Fig. 1C) [28,29], the sum of intensities significantly increased on PLL coated quartz versus uncoated controls as expected (Fig. 2D; +2.23 and +4.26-fold respectively). Following the calculation of the area ratio of hydroxyproline to proline, reflecting the strength of the intra-strand bonds between these residues in collagen, an unsurprising increase was noted on PLL coated quartz versus controls (Fig. 2E; +1.68 and +1.38-fold respectively), indicating that the collagen triple helix is more tightly held together and mature under these conditions.

The transient precursors of mature crystalline bone mineral, namely ACP (948 cm^{-1}), OCP (970 cm^{-1}) and CAP (959 cm^{-1}) were also detected. As a function of the total phosphates (940 cm^{-1} to 980 cm^{-1}), levels of ACP were significantly higher in OBs cultured in basal (Fig. 2F; +1.89-fold) and osteogenic medium (+1.91-fold) on PLL coatings compared to the uncoated controls. Conversely OCP was reduced in OBs cultured in basal medium on PLL coated quartz versus uncoated controls (Fig. 2G; -1.56-fold) yet significantly increased in cultures supplemented with osteogenic medium (+1.6 fold). The largest fold reduction was observed in CAP produced by OBs on PLL coated quartz versus the respective uncoated controls (Fig. 2H; -4.77 and -9.32-fold respectively). The mineral/matrix ratio calculated by the area ratio of CAP to proline, detailing overall mineralization ability was significantly decreased in OB cultures on PLL coated quartz compared to uncoated controls (Fig. 2I; -1.65 and -33.54-fold respectively), demonstrating that a mature mineralizing OB signature can only be obtained in vitro through culture on uncoated quartz in osteogenic medium. Collectively, this univariate analysis of these Raman spectra indicates that the mineralization of the ECM is not sufficiently achieved in the presence of PLL. These findings were complemented by the clustering of scores observed following the application of principle component analysis (PCA) on the collected Raman spectra from each condition (Fig. S3A). PC1 is comprised of the highest variation (40.3%) between conditions and primarily accounted by ACP and CAP as seen in the loadings. The evaluation of the PC clustering values indicated similarity between the scores for the basal uncoated (mean score = -0.001582) and osteogenic coated group (mean score = -0.0001143) which are consistent with the findings of the spectral deconvolution analysis (Fig. 2F and H). PC2 and PC3 accounted for 28.9% and 9.72% of the spectral variation respectively (Fig. S3A). Although contributing less variation, PC2 consists of

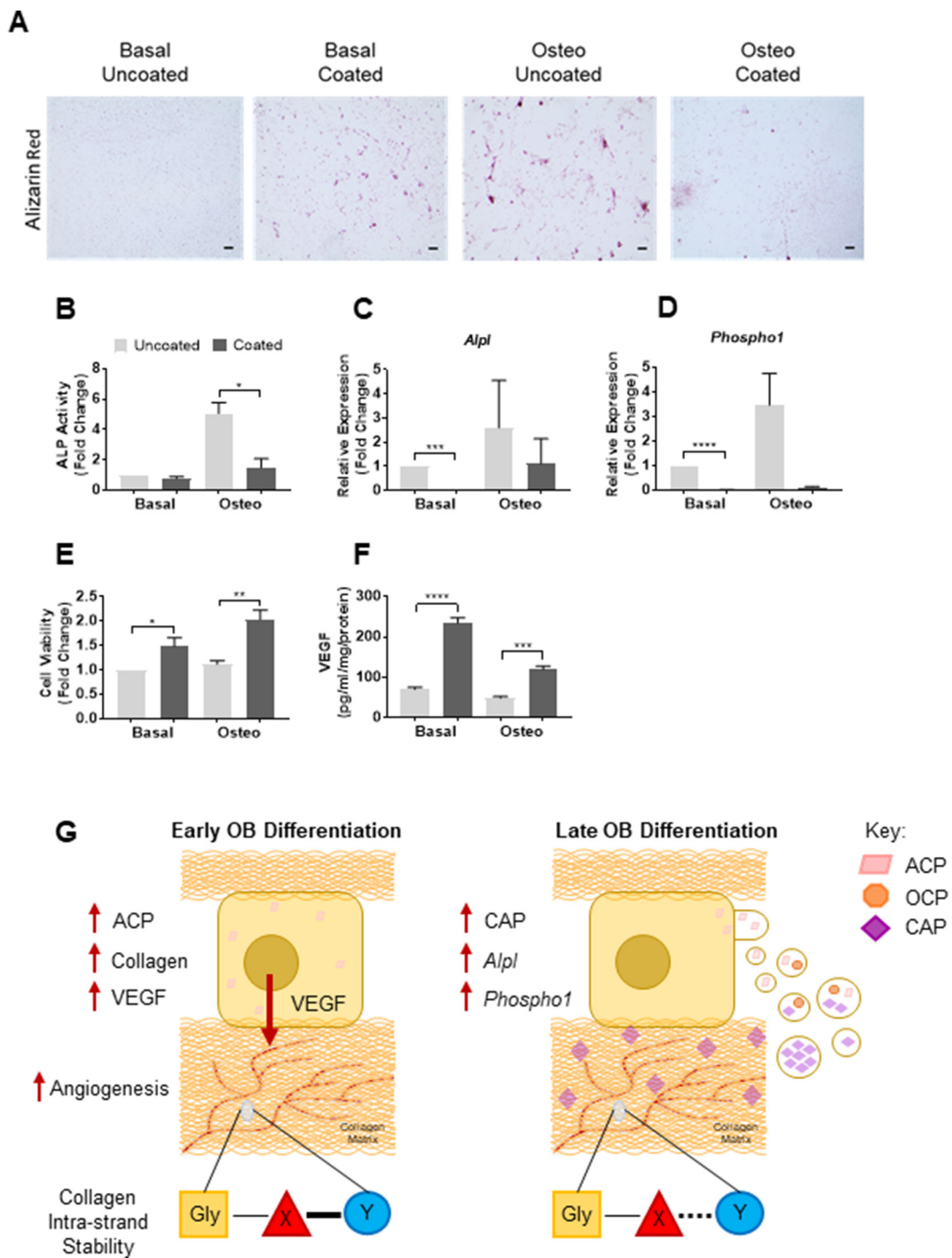


Fig. 3. PLL inhibits OB differentiation but increases cell viability and angiogenic potential. Reduced Alizarin Red staining of mineral deposits (scale bars represent 250 μ m), was observed in 19-day OB cultures on PLL coated quartz (A). Enzymatic alkaline phosphatase (ALP) activity (B) and OB mRNA expression levels of *Alpl* (C) and *Phospho1* (D) similarly decreased on PLL coated quartz. Increased OB viability was observed on PLL coated quartz versus uncoated controls (E). OB-derived VEGF release was elevated on PLL coating versus uncoated controls (F). Data represent mean values \pm SEM from three separate experiments. Statistical significance between groups was assessed using Student's *t*-test ($P < .05^*$, $P < .01^{**}$, $P < .001^{***}$, $P < .0001^{****}$). Schematic summarizing the effects of PLL coating of quartz on osteogenic differentiation and angiogenic capacity (G).

intermediate metastable phases existing between CAP and OCP (959 cm^{-1} to 980 cm^{-1}) [25,30]. These subtle differences in PC2 however, allow discrimination between basal and osteogenic conditions, with basal uncoated and basal coated clustering at mean score = -0.0002549 and -0.001717 respectively versus osteogenic uncoated, mean score = 0.001922 , and osteogenic coated, mean score = 0.002317 . While the distinction is possible between the various conditions, PC2 and PC3 loadings consist of overlapping contributions from OCP and CAP and hence, do not correlate well to the peak analysis results of the deconvolution (Fig. 2G and H).

PLL inhibits osteoblastic calcium phosphate deposition and downregulates matrix mineralization genes

To establish the functional effect of PLL on osteogenic differentiation potential, OB cultures were stained with Alizarin Red, widely used in the literature to assess the extent of matrix mineralization [31–33] and moreover, to assess the effects on calcium phosphate deposition. In the present study, Alizarin Red staining was found to be reduced on PLL coated substrates versus uncoated controls (Fig. 3A). As expected, an increase in staining was observed on uncoated quartz between cultures in basal and osteogenic medium (Fig. 3A). These findings were further supported following the assessment of enzymatic alkaline phosphatase (ALP) activity, conducted in tandem with gene expression analysis (Fig. 3B–D). PLL was shown to significantly decrease ALP activity in OB cultures on PLL coated quartz (Fig. 3C; -0.8 and -3.38 -fold respectively) compared to uncoated controls. In addition, a downregulation of markers associated with a mineralizing population of OBs, namely *Alpl* (Fig. 3C; -55.17 and -2.32 -fold respectively) and *Phospho1* (Fig. 3D; -57.8 and 28.8 -fold respectively) were observed on PLL coated quartz compared to uncoated controls.

Cell viability and angiogenic potential of osteoblasts is increased with PLL

To determine if PLL coating of the quartz coverslips had a detrimental effect on the OBs, an ATP luminescent cell viability assay was performed. Surprisingly, a significant increase in cell viability (Fig. 3E) was observed on PLL coatings compared to uncoated controls ($+1.48$ and $+1.82$ -fold respectively), suggesting that an increase in adhesion to the quartz supported and increased cellular integrity. Finally, to assay the ability of the OBs cultured on uncoated or PLL coated quartz to produce angiogenic factors, specifically VEGF, a VEGF-A ELISA of the collected conditioned media

was conducted. In vitro and in vivo studies have shown OBs are producers of angiogenic factors and signal to endothelial cells in a paracrine manner [34–38]. In the present study, VEGF concentration in the OB-conditioned media was significantly raised in cultures on PLL coated quartz versus control (Fig. 3F; $+3.33$ and $+2.46$ -fold respectively), together correlating with higher cell viability levels.

Discussion

The mineralization of the ECM by OBs is carefully orchestrated and essential for the maturation of the osteoid into mature bone [5,6,11,39]. Occurring through a biphasic process, the initial accumulation of mineral species is thought to be regulated by an abundance of factors and molecules that are concentrated within MVs extracellularly. Examples include the balance between pyrophosphate and inorganic phosphate, ALP, ecto-nucleotide pyrophosphatase/phosphodiesterase-1 (NPP1) and PHOSPHO1 in addition to the ankylosis protein (ANK) [5,6,11,12,39–44]. Gaps remain in our knowledge regarding the mechanisms controlling the key steps of mineralization initiation and its subsequent coupling to blood vessel growth. To address this we have successfully utilized Raman spectroscopy to define stages in OB maturation by investigating the association of ECM spectral signatures with pro-angiogenic VEGF levels.

To inspect the effect of PLL on collagen production, proline and hydroxyproline bands were selected as suitable markers of type I collagen content and quality as described in previous Raman analyses [29,45]. In greater detail, the present study showed that culture of OBs on PLL yielded increased levels of proline and hydroxyproline species which correlated with the additional elevations in ACP and lack of CAP. Thus, PLL has the potential to reduce the maturation ability of OBs by inhibiting their ability to mineralize, and instead, promotes collagen deposition associated with the pre-mineralization phases of OB differentiation [46] characterized by an immature matrix signature. These specific changes were corroborated by detection of reduced ALP enzymatic activity, *Alpl* and *Phospho-1* mRNA levels and Alizarin Red staining. The resultant alterations to the OB ECM composition by the PLL coating is reinforced as the converse effect was observed on uncoated substrates even in the absence of osteogenic medium, where elevated CAP and reduced ACP and collagen species levels were detected. We also found that the hydroxyproline/proline ratio, calculated by the area ratio of the 876 cm^{-1} peak to 853 cm^{-1} detailing the intra-strand stability of the collagen triple helix [29] was considerably higher in

OB cultures on PLL substrates. Another recognized metric calculated in Raman spectroscopic studies and frequently used in the quantification of components of bone and bone quality is the mineral/matrix ratio. In the current study, this was used to assess both the ability and capacity of OBs to mineralize the ECM [47,48]. Calculated by the area ratio of $\nu_1\text{PO}_4^{3-}$ (959 cm^{-1}) peak for CAP to that of proline (853 cm^{-1}), hydroxyproline (876 cm^{-1} , data not shown) and their sum (data not shown), we observed that the mineral/matrix ratio was considerably reduced in the presence of PLL, due to the larger quantities of collagen species in comparison to CAP.

Mechanistically, our current findings support known modes of osteoblastic matrix and mineral deposition [5,6,11,12,40–43,49]. The observed lack of CAP and increased collagen intra-strand stability on PLL indicates that the mineralization capacity of OBs is premature, despite reports that suggest increased hydroxylation of proline promotes apatite binding [50]. We showed that PLL supports ECM deposition by promoting the post-translational modification of proline, to produce hydroxyproline yet reduces progression to the sequential stages of OB differentiation whereby the production and release of mineral species is predominant. If the gap junctions of collagen serve as mineral nucleation sites, once occupied, the collagen-intra-strand stability should thereby reduce to accommodate the deposition of new mineral, possibly occurring concomitantly to initial ECM deposition. Collectively, the current study has demonstrated utility of Raman spectroscopic analyses for the definition of unique spectral markers of mineral and collagenous matrix composition. Furthermore, the additional label-free and non-destructive nature of the modality highlights and endorses its potential for rapid in vitro assessment of OB performance and maturational status.

An unexpected finding of our study was that the restriction of mature CAP by OBs on PLL was associated with increased OB viability and VEGF release. Early OB-derived VEGF has previously been shown to play a critical role in bone development and fracture repair [34,35,51]. Furthermore, it has been identified that early OBs interact specifically with the vasculature in contrast to more mature OBs to regulate VEGF production [52]. Together, our data supports the idea that early OB VEGF release occurs alongside matrix deposition and the use of PLL may promote a pro-angiogenic environment allowing for blood vessel formation ahead of mineralization.

PLL coating of coverslips have been used in the past for the study of OB function by providing a positively charged basic amino acid to improve cell adhesion to facilitate cell study [53–55]. It has previously been reported that PLL promotes attachment and cell spreading of primary bone cells and

OB-like cell lines [55–59], endothelial cells [60], cancer cells [61] and stem cells [62–66] through the electrostatic attraction between the positively charged PLL residues and the negatively charged phospholipids on the cell membrane. Despite the use of PLL in these previous studies, the effect on the differentiation potential of OBs remains inconclusive due to a lack of validation in vitro regarding the impact of PLL on mineralization. The focus of previous work was to improve cell adhesion on 3D scaffolds in vitro, ahead of in vivo implantation with PLL applied as a surface coating. Complementing our findings, similar morphological changes and improvements in cell viability were reported [55,59,65,67]. However, in contrast, increases in the expression of osteogenic genes alongside enhanced ALP enzymatic activity were evident with higher concentrations of PLL of 0.1 mg/ml or greater. It is possible that such discrepancies in our results are driven by the concentration and/or the unique effects of PLL on 3D scaffolds and therefore highlights the necessity to robustly characterize the implications of PLL on OB mineralization on a range of substrates. Buo et al. [68] have also recently reported that PLL can improve adenoviral infection efficiency in OB-like cells. This effect may be due to the captivation of OBs within a proliferative phase when on PLL hence promoting viral uptake. However the impact on mineralization was not investigated and our results continue to question the usefulness of PLL coating for inducing OB adenoviral infection in the context of restricting mineralization.

In summary, the present study has identified that OB maturation and ability to participate in matrix mineralization is restricted when cultured on substrates coated with PLL. Raman spectroscopy identified that this restriction in differentiation reduces the mineral/matrix ratio since the ECM was predominantly comprised of the immature mineral, ACP, partnered with an abundance of collagen specific species. Furthermore, we observed a pronounced increase in the collagen intra-strand stability by PLL, which in combination with the shift in mineral species and availability of collagen components is suggestive of compromised mineral nucleation ability within the OB ECM. This correlated with reduced ALP enzymatic activity, Alizarin Red staining in addition to *Alpl* and *Phospho-1* mRNA levels however increased VEGF production and cell viability were evident. In contrast, OB maturation was enhanced in the absence of PLL where the reversed effects were observed.

Our study reiterates that label-free vibrational methods such as Raman spectroscopy offer significant potential in the field of matrix biology and for disease diagnosis given their enhanced sensitivity to changes, complementary information content and non-destructive nature. Our existing knowledge of disorders of bone mineralization

including; rickets, tumor-induced osteomalacia, hypophosphatasia, McCune-Albright syndrome, and osteogenesis imperfecta have primarily accumulated through genetic studies, histological analysis, and computed tomography. However sensitively probing specific components of the bone may yield additional information regarding bone compositional quality. As the degree of bone mineralization has also been reported to be a determinant of bone strength [69,70], the elucidation of a bone specific matrix signature is now of critical importance as is defining the underlying molecular signals. Relating OB matrix signatures to angiogenic capacity and viability in vitro could therefore provide a unique template signature allowing degree of mineralization to be assessed clinically with implications for an ageing demographic.

Methodology

Materials

Cell culture reagents, such α -Minimum Essential Medium (α MEM; no. 41061) and fetal bovine serum (FBS; no. 102701) were purchased from Gibco (Paisley, UK). All other cell culture reagents were obtained from Merck (Gillingham, UK) unless otherwise stated.

Isolation and culture of osteoblasts

All studies involving the use of mice were conducted under the regulations set by the UK Home Office and in accordance with the United Kingdom Animals (Scientific Procedures) Act of 1986. Primary murine long bone OBs were obtained from P4 C57BL/6 mice by the collagenase-collagenase-EDTA-collagenase (CCEC) extraction method as previously described [33]. Briefly, the long bones, namely the tibia, fibula and femur were isolated and washed in Hanks Balanced Salt Solution (HBSS) prior to being incubated in 1 mg/ml collagenase type II (Worthington Biochemical Cooperation, USA) reconstituted in HBSS for 10 min at 37 °C. The supernatant of the first digest was not retained. The second fraction; obtained by repeat digestion with 1 mg/ml collagenase type II for 30 min, third fraction; 4 mM EDTA for 10 min and fourth fraction; 1 mg/ml collagenase type II for 30 min, all at 37 °C, were retained and combined. Cells were resuspended in basal α MEM consisting of 10% heat-inactivated FBS, 0.1% gentamicin, 100 U/ml penicillin, 100 μ g/ml streptomycin before being cultured in 75 cm² flasks and incubated at 37 °C/5% CO₂ until 80% confluent. Medium was replenished twice weekly.

Upon confluence, OBs were either plated onto uncoated or poly-L-lysine (PLL; 50 μ g/ml, 30,000–70,000 Mw) coated quartz coverslips (#No5, thickness: 0.5 mm, \varnothing 20; UQG-Optics, UK) in 12-well plates at a density of 10,000 cells per well. Coverslips were firstly sterilized in 100% ethanol before being incubated in PLL solution or sterile distilled water for 2 h at 37 °C prior to UV irradiation ahead of cell plating. After plating, OBs were left to adhere for 2 days before being treated with basal or osteogenic (osteo) α MEM medium containing 10% FBS, 2 mM β -glycerophosphate and 50 μ g/ml L-ascorbic acid to stimulate differentiation in vitro. Culture medium was replenished every 3 days until day 19 of culture, unless otherwise stated.

Raman spectroscopy

OBs were briefly washed with PBS prior to fixation with 4% paraformaldehyde (PFA) in preparation ahead of spectral acquisition as both the suitability of PFA fixation has been validated [71–74] and widespread use is documented in several studies [25,75–78]. Raman spectra were obtained using a Renishaw® inVia Raman microscope equipped with a 532 nm laser with a Gaussian beam profile and a Leica 63 \times water-immersion microscope objective with a numerical aperture of 1.2 as previously described [25]. The instrument was internally calibrated to the 520.7 cm⁻¹ peak of silicon for wavenumber and intensity calibration ahead of spectral acquisition. Raman spectra were collected using single point static scans, with an exposure of 20 s, 100% laser power and 3 accumulations within the “Fingerprint region” from 800 cm⁻¹ to 1750 cm⁻¹ [79]. The laser power on the sample was approximately 30 mW with the calculated diffraction limited spot size being approximately 280 nm. From each preparation, spectra were collected from 5 points within the cytoplasmic region of 25 cells to minimise both spatial and spectral heterogeneity between samples and conditions. We have previously identified a range of vibrations corresponding to collagen and the ECM [25] such as proline (853 cm⁻¹), hydroxyproline (876 cm⁻¹) and those associated with mineral such as ν_1 PO₄³⁻ (959 cm⁻¹) and other weaker bands between 940 cm⁻¹ and 980 cm⁻¹ which were similarly identified in the present study (Fig. 1B and S2A). Cosmic ray artefacts upon acquisition and background contributions from quartz (Fig. S1A) were removed from raw spectra (Fig. S1B) using WiRE 4.1. Further analysis involved the utilisation of iRootLab [80], whereby spectra were pre-processed before further analysis. They were wavelet denoised (Haar wavelets, 6-point smoothing), background corrected by the fitting of a 9th order polynomial and vector normalized (Fig. S2B). Vector normalization

is essential to allow comparison of intensities in the spectra between different treatments. The second order derivative (Fig. S2C) was calculated ahead of univariate spectral deconvolution to obtain various peak parameters, in which a mixture of Lorentzian and Gaussian curves were fitted to the regions of interest (Fig. S2A). Peak area was extracted by fitting of the relevant spectral regions of the class mean spectra (Fig. S2D) using WiRE 4.1 as previously described [25]. Typically, 3 to 6 peaks were fitted per spectral region until the fitting returned an R^2 value lower than 1. For multivariate analysis, PCA was performed on the denoised and background corrected Raman spectra following mean-centring in iRootLab [80] (Fig. S3A).

Alkaline phosphatase analysis

OBs were washed with PBS prior to fixation in 100% ethanol for 2 min. After washing with distilled water, cells were incubated in a working solution consisting of 70% distilled water, 20% 0.1 M NaHCO_3 and 10% 30 mM MgCl_2 with 1 mg/ml P-nitrophenol phosphate disodium salt (Merck, UK) for 30 min at 37 °C as described in the literature [25,38]. Two hundred μl of the eluted solution was transferred to a 96-well plate in duplicates and absorbance was measured at 405 nm against P-nitrophenol standards of known concentration.

Alizarin Red staining

Cultured OBs were prepared for staining by washing with PBS prior to fixation in ice cold acetone: methanol (1:1) for 2 min followed by washes in distilled water. Fixed cells were incubated in 2% Alizarin Red staining solution with pH 4.5 and incubated at room temperature in the dark for 45 min.

Cell viability

OBs plated on uncoated or PLL coated quartz coverslips were left to adhere for 2 days before being treated with basal or osteogenic medium for 24 h. After this, cell viability measured in luminescence was quantified using the CellTiter-Glo® Viability Assay Kit (Promega, UK) following cell incubation with the CellTiter-Glo® reagent for 10 min at room temperature using a GloMax®-Multi+ Detection System (Promega, UK).

Collection of conditioned medium and VEGF ELISA

OBs plated on uncoated or PLL coated quartz coverslips were cultured in basal or osteogenic medium until day 18 of culture. On day 18, following the removal of the culture medium, cells were

“stepped down” in low serum media (1% FBS) for 24 h ahead of collection on day 19. A VEGF-A mouse sandwich ELISA kit and reagents (R&D Systems, USA) were used to quantify natural and recombinant VEGF (VEGF₁₂₀ and VEGF₁₆₄) in the collected conditioned media following the manufacturers instruction.

Reverse transcription-quantitative PCR (RT-qPCR)

RNA from the cultured OBs were isolated from each preparation using the Monarch® Total RNA Miniprep Kit (New England Biolabs, UK) following the manufacturers instruction. Five hundred ng of RNA per condition was reverse transcribed using the LunaScript® RT Supermix (New England Biolabs, UK) as per the manufacturer's recommendation. RT-qPCR of reactions containing 25 ng cDNA, 250 mM forward and reverse primers (Primerdesign, UK) and PrecisionPlus mastermix was carried out in the StepOnePlus Real-Time PCR System (Applied Biosystems, UK). Primer sequences are as follows, *Alpl*; forward; 5'-TTCTCATTTCGGATGCCAAC-3' and reverse; 3'-TTCTCATTTCGATGCCAAC-5', *Phospho1*; forward 5'-GGGACGAATCTCAGGGTACA-3' and reverse; 3'-AGTAACTGGGGTCTCTCTCTTT-5'. Ct values were normalized to that of *Atp5b* (Primerdesign, UK) [4,81–83] and relative expression was calculated using the $\Delta\Delta\text{Ct}$ method as described in the literature [84].

Statistical analysis

Data is expressed as the mean value \pm standard error of the mean (SEM). Cells used in experiments were isolated from $n = 6$ mice from at least three independent litters. Statistical analysis was performed by Student's *t*-test. $P < .05$ was considered to be statistically significant and is noted as *. P values of $< .01$, $< .001$ and $< .0001$ are denoted **, *** and **** respectively.

Declaration of competing interest

None.

Acknowledgements

This study was kindly funded by the School Biological Sciences, University of Southampton, UK and DOT Medical Implant Solutions, Germany.

Appendix A. Supplementary data

Supplementary data to this article can be found online at <https://doi.org/10.1016/j.mbsplus.2019.100018>.

Received 1 May 2019;

Received in revised form 21 August 2019;

Accepted 9 October 2019

Available online 20 November 2019

Keywords:

Raman spectroscopy;
Poly-L-lysine;
Osteoblast mineralization;
VEGF

Abbreviations used:

ACP, amorphous calcium phosphate; ALP, tissue non-specific alkaline phosphatase; OB, osteoblast; CAP, carbonated apatite; CCEC, collagenase-collagenase-EDTA-collagenase; ECM, extracellular matrix; HA, hydroxyapatite; HBSS, Hank's balanced salt solution; MV, matrix vesicles; OCP, octacalcium phosphate; PCA, principle component analysis; PLL, poly-L-lysine; RT-qPCR, reverse transcription-quantitative PCR; VEGF, vascular endothelial growth factor.

References

- [1] B. Javaheri, A. Carriero, K.A. Staines, Y.M. Chang, D.A. Houston, K.J. Oldknow, J.L. Millan, B.N. Kazeruni, P. Salmon, S. Shefelbine, C. Farquharson, A.A. Pitsillides, Phospho1 deficiency transiently modifies bone architecture yet produces consistent modification in osteocyte differentiation and vascular porosity with ageing, *Bone* (2015) <https://doi.org/10.1016/j.bone.2015.07.035>.
- [2] S. Roberts, S. Narisawa, D. Harmey, J.L. Millán, C. Farquharson, Functional involvement of PHOSPHO1 in matrix vesicle-mediated skeletal mineralization, *J. Bone Miner. Res.* 22 (2007) 617–627, <https://doi.org/10.1359/jbmr.070108>.
- [3] C. Huesa, D. Houston, T. Kiffer-Moreira, M.C. Yadav, J. Luis Millan, C. Farquharson, The functional co-operativity of tissue-nonspecific alkaline phosphatase (TNAP) and PHOSPHO1 during initiation of skeletal mineralization, *Biochem. Biophys. Reports* 4 (2015) 196–201, <https://doi.org/10.1016/j.bbrep.2015.09.013>.
- [4] C. Huesa, D. Zhu, J.D. Glover, M. Ferron, G. Karsenty, E.M. Milne, J.L. Millan, S.F. Ahmed, C. Farquharson, N.M. Morton, V.E. MacRae, Deficiency of the bone mineralization inhibitor NPP1 protects mice against obesity and diabetes, *Dis. Model. Mech.* (2014) <https://doi.org/10.1242/dmm.017905>.
- [5] K.A. Staines, D. Zhu, C. Farquharson, V.E. MacRae, Identification of novel regulators of osteoblast matrix mineralization by time series transcriptional profiling, *J. Bone Miner. Metab.* (2014) <https://doi.org/10.1007/s00774-013-0493-2>.
- [6] K.A. Staines, V.E. MacRae, C. Farquharson, The importance of the SIBLING family of proteins on skeletal mineralisation and bone remodelling, *J. Endocrinol.* (2012) <https://doi.org/10.1530/joe-12-0143>.
- [7] H.C. Anderson, D. Harmey, N.P. Camacho, R. Garimella, J. B. Sipe, S. Tague, X. Bi, K. Johnson, R. Terkeltaub, J.L. Millán, Sustained osteomalacia of long bones despite major improvement in other hypophosphatasia-related mineral deficits in tissue nonspecific alkaline phosphatase/nucleotide pyrophosphatase phosphodiesterase 1 double-deficient mice, *Am. J. Pathol.* (2005) [https://doi.org/10.1016/S0002-9440\(10\)62481-9](https://doi.org/10.1016/S0002-9440(10)62481-9).
- [8] S. Narisawa, M.C. Yadav, J.L. Millán, In vivo overexpression of tissue-nonspecific alkaline phosphatase increases skeletal mineralization and affects the phosphorylation status of osteopontin, *J. Bone Miner. Res.* (2013) <https://doi.org/10.1002/jbmr.1901>.
- [9] N.J. Crane, V. Popescu, M.D. Morris, P. Steenhuis, M.A. Ignelzi Jr., Raman spectroscopic evidence for octacalcium phosphate and other transient mineral species deposited during intramembranous mineralization, *Bone* 39 (2006) 434–442, <https://doi.org/10.1016/j.bone.2006.02.059>.
- [10] C.P. Tamowski, M.A. Ignelzi Jr., M.D. Morris, Mineralization of developing mouse calvaria as revealed by Raman microspectroscopy, *J. Bone Min. Res.* 17 (2002) 1118–1126, <https://doi.org/10.1359/jbmr.2002.17.6.1118>.
- [11] S. Boonrungsiman, E. Gentleman, R. Carzaniga, N.D. Evans, D.W. McComb, A.E. Porter, M.M. Stevens, The role of intracellular calcium phosphate in osteoblast-mediated bone apatite formation, *Proc. Natl. Acad. Sci.* (2012) <https://doi.org/10.1073/pnas.1208916109>.
- [12] E.E. Golub, Role of matrix vesicles in biomineralization, *Biochim. Biophys. Acta - Gen. Subj.* (2009) <https://doi.org/10.1016/j.bbagen.2009.09.006>.
- [13] F. Nudelman, K. Pieterse, A. George, P.H.H. Bomans, H. Friedrich, L.J. Brylka, P.A.J. Hilbers, G. de With, N. Sommerdijk, The role of collagen in bone apatite formation in the presence of hydroxyapatite nucleation inhibitors, *Nat. Mater.* 9 (2010) 1004–1009, <https://doi.org/10.1038/nmat2875>.
- [14] E. Bonucci, The origin of matrix vesicles and their role in the calcification of cartilage and bone, *Int. Cell Biol.* 1980–1981 (2013) https://doi.org/10.1007/978-3-662-39932-3_111.
- [15] A.J. Stewart, S.J. Roberts, E. Seawright, M.G. Davey, R.H. Fleming, C. Farquharson, The presence of PHOSPHO1 in matrix vesicles and its developmental expression prior to skeletal mineralization, *Bone*. (2006) <https://doi.org/10.1016/j.bone.2006.05.014>.
- [16] G.J. Puppels, F.F.M. Demul, C. Otto, J. Greve, M. Robertnicoud, D.J. Arndtjovin, T.M. Jovin, Studying single living cells and chromosomes by confocal Raman microspectroscopy, *Nature*. 347 (1990) 301–303, <https://doi.org/10.1038/347301a0>.
- [17] P.S. Hung, Y.C. Kuo, H.G. Chen, H.H.K. Chiang, O.K.S. Lee, Detection of osteogenic differentiation by differential mineralized matrix production in mesenchymal stromal cells by Raman spectroscopy, *PLoS One* (2013) <https://doi.org/10.1371/journal.pone.0065438>.
- [18] Q. Tu, C. Chang, Diagnostic applications of Raman spectroscopy, nanomedicine nanotechnology, *Biol. Med.* (2012) <https://doi.org/10.1016/j.nano.2011.09.013>.
- [19] R. Smith, K.L. Wright, L. Ashton, Raman spectroscopy: an evolving technique for live cell studies, *Analyst.* (2016) <https://doi.org/10.1039/c6an00152a>.
- [20] M.J. Pelletier, Quantitative analysis using Raman spectrometry, *Appl. Spectrosc.* (2003) <https://doi.org/10.1366/000370203321165133>.
- [21] Y. Kumamoto, Y. Harada, T. Takamatsu, H. Tanaka, Label-free Molecular Imaging and Analysis by Raman

- Spectroscopy, ACTA Histochem, Cytochem, 2018 <https://doi.org/10.1267/ahc.18019>.
- [22] C.C. Moura, R.S. Tare, R.O.C. Oreffo, S. Mahajan, Raman spectroscopy and coherent anti-Stokes Raman scattering imaging: prospective tools for monitoring skeletal cells and skeletal regeneration, *J. R. Soc. Interface* 13 (2016) 12, <https://doi.org/10.1098/rsif.2016.0182>.
- [23] M. Raghavan, N.D. Sahar, R.H. Wilson, M.-A. Mycek, N. Pleshko, D.H. Kohn, M.D. Morris, Quantitative polarized Raman spectroscopy in highly turbid bone tissue, *J. Biomed. Opt.* (2010) <https://doi.org/10.1117/1.3426310>.
- [24] D.W. Shipp, F. Sinjab, I. Notingher, Raman spectroscopy: techniques and applications in the life sciences, *Adv. Opt. Photonics*. (2017) <https://doi.org/10.1364/aop.9.000315>.
- [25] S.J. Smith, R. Emery, A. Pitsillides, C.E. Clarkin, S. Mahajan, Detection of early osteogenic commitment in primary cells using Raman spectroscopy, *Analyst*. (2017) <https://doi.org/10.1039/c6an02469f>.
- [26] M.J. Glimcher, The nature of the mineral component of bone and the mechanism of calcification, *Instr. Course Lect.* 36 (1987) 49–69.
- [27] H.P. Schwarcz, E.A. McNally, G.A. Botton, Dark-field transmission electron microscopy of cortical bone reveals details of extrafibrillar crystals, *J. Struct. Biol.* (2014) <https://doi.org/10.1016/j.jsb.2014.10.005>.
- [28] M.D. Shoulders, R.T. Raines, Collagen structure and stability, *Annu. Rev. Biochem.* (2009) <https://doi.org/10.1146/annurev.biochem.77.032207.120833>.
- [29] C. Olejnik, G. Falgayrac, A. During, B. Cortet, G. Penel, Doses effects of zoledronic acid on mineral apatite and collagen quality of newly-formed bone in the rat's calvaria defect, *Bone*. (2016) <https://doi.org/10.1016/j.bone.2016.05.002>.
- [30] A. Lotsari, A.K. Rajasekharan, M. Halvarsson, M. Andersson, Transformation of amorphous calcium phosphate to bone-like apatite, *Nat. Commun.* (2018) <https://doi.org/10.1038/s41467-018-06570-x>.
- [31] C.A. Gregory, W.G. Gunn, A. Peister, D.J. Prockop, An Alizarin red-based assay of mineralization by adherent cells in culture: comparison with cetylpyridinium chloride extraction, *Anal. Biochem.* (2004) <https://doi.org/10.1016/j.ab.2004.02.002>.
- [32] S.E.B. Taylor, M. Shah, I.R. Orriss, Generation of rodent and human osteoblasts, *Bonekey Rep.* 3 (2014) 585, <https://doi.org/10.1038/bonekey.2014.80>.
- [33] I.R. Orriss, M.O. Hajjawi, C. Huesa, V.E. MacRae, T.R. Arnett, Optimisation of the differing conditions required for bone formation in vitro by primary osteoblasts from mice and rats, *Int. J. Mol. Med.* 34 (2014) 1201–1208, <https://doi.org/10.3892/ijmm.2014.1926>.
- [34] K. Hu, B.R. Olsen, The roles of vascular endothelial growth factor in bone repair and regeneration, *Bone*. 91 (2016) 30–38, <https://doi.org/10.1016/j.bone.2016.06.013>.
- [35] K. Hu, B.R. Olsen, Osteoblast-derived VEGF regulates osteoblast differentiation and bone formation during bone repair, *J. Clin. Invest.* 126 (2016) 509–526, <https://doi.org/10.1172/jci82585>.
- [36] A.D. Berendsen, B.R. Olsen, How vascular endothelial growth factor-A (VEGF) regulates differentiation of mesenchymal stem cells, *J. Histochem. Cytochem.* 62 (2014) 103–108, <https://doi.org/10.1369/0022155413516347>.
- [37] Y. Liu, A.D. Berendsen, S. Jia, S. Lotinun, R. Baron, N. Ferrara, B.R. Olsen, Intracellular VEGF regulates the balance between osteoblast and adipocyte differentiation, *J. Clin. Invest.* 122 (2012) 3101–3113, <https://doi.org/10.1172/jci61209>.
- [38] C.E. Clarkin, R.J. Emery, A.A. Pitsillides, C.P. Wheeler-Jones, Evaluation of VEGF-mediated signaling in primary human cells reveals a paracrine action for VEGF in osteoblast-mediated crosstalk to endothelial cells, *J. Cell. Physiol.* 214 (2008) 537–544, <https://doi.org/10.1002/jcp.21234>.
- [39] L. Cui, D.A. Houston, C. Farquharson, V.E. MacRae, Characterisation of matrix vesicles in skeletal and soft tissue mineralisation, *Bone*. (2016) <https://doi.org/10.1016/j.bone.2016.04.007>.
- [40] H. Orimo, The mechanism of mineralization and the role of alkaline phosphatase in health and disease, *J. Nippon Med. Sch.* (2010) <https://doi.org/10.1272/jnms.77.4>.
- [41] T. Hasegawa, T. Yamamoto, E. Tsuchiya, H. Hongo, K. Tsuboi, A. Kudo, M. Abe, T. Yoshida, T. Nagai, N. Khadiza, A. Yokoyama, K. Oda, H. Ozawa, P.H.L. de Freitas, M. Li, N. Amizuka, Ultrastructural and biochemical aspects of matrix vesicle-mediated mineralization, *Jpn. Dent. Sci. Rev.* (2017) <https://doi.org/10.1016/j.jdsr.2016.09.002>.
- [42] H.C. Anderson, Matrix vesicles and calcification, *Curr. Rheumatol. Rep.* (2003) <https://doi.org/10.1007/s11926-003-0071-z>.
- [43] H.C. Anderson, Molecular biology of matrix vesicles, *Clin. Orthop. Relat. Res.* (2006) <https://doi.org/10.1097/00003086-199505000-00034>.
- [44] C. Wang, Y. Wang, N.T. Huffman, C. Cui, X. Yao, S. Midura, R.J. Midura, J.P. Gorski, Confocal laser Raman microspectroscopy of biomineralization foci in UMR 106 osteoblastic cultures reveals temporally synchronized protein changes preceding and accompanying mineral crystal deposition, *J. Biol. Chem.* (2009) <https://doi.org/10.1074/jbc.M805898200>.
- [45] I.A. Karampas, M.G. Orkoulas, C.G. Kontoyannis, A quantitative bioapatite/collagen calibration method using Raman spectroscopy of bone, *J. Biophotonics* (2013) <https://doi.org/10.1002/jbio.201200053>.
- [46] Y.T. Tsao, Y.J. Huang, H.H. Wu, Y.A. Liu, Y.S. Liu, O.K. Lee, Osteocalcin mediates biomineralization during osteogenic maturation in human mesenchymal stromal cells, *Int. J. Mol. Sci.* (2017) <https://doi.org/10.3390/ijms18010159>.
- [47] M.D. Morris, G.S. Mandair, Raman assessment of bone quality, *Clin. Orthop. Relat. Res.* 469 (2011) 2160–2169, <https://doi.org/10.1007/s11999-010-1692-y>.
- [48] G.S. Mandair, M.D. Morris, Contributions of Raman spectroscopy to the understanding of bone strength, *Bonekey Rep.* 4 (2015) 8, <https://doi.org/10.1038/bonekey.2014.115>.
- [49] W. Yang, D. Guo, M.A. Harris, Y. Cui, J. Gluhak-Heinrich, J. Wu, X.-D. Chen, C. Skinner, J.S. Nyman, J.R. Edwards, G.R. Mundy, A. Lichtler, B.E. Cream, D.W. Rowe, I. Kalajzic, V. David, D.L. Quarles, D. Villareal, G. Scott, M. Ray, S. Liu, J.F. Martin, Y. Mishina, S.E. Harris, Bmp2 in osteoblasts of periosteum and trabecular bone links bone formation to vascularization and mesenchymal stem cells, *J. Cell Sci.* 126 (2013) 4085–4098, <https://doi.org/10.1242/jcs.118596>.
- [50] N. Almora-Barrios, K.F. Austen, N.H. De Leeuw, Density functional theory study of the binding of glycine, proline, and hydroxyproline to the hydroxyapatite (0001) and (0110) surfaces, *Langmuir*. (2009) <https://doi.org/10.1021/la803842g>.
- [51] A.D. Berendsen, Y. Liu, Y. Murata, B.R. Olsen, X. Duan, C. Nicolae, Vegfa regulates perichondrial vascularity and osteoblast differentiation in bone development, *Development*. (2015) <https://doi.org/10.1242/dev.117952>.

- [52] C. Maes, T. Kobayashi, M.K. Selig, S. Torrekens, S.I. Roth, S. Mackem, G. Carmeliet, H.M. Kronenberg, Osteoblast precursors, but not mature osteoblasts, move into developing and fractured bones along with invading blood vessels, *Dev. Cell* (2010) <https://doi.org/10.1016/j.devcel.2010.07.010>.
- [53] D. Carrier, M. Pérolet, Raman spectroscopic study of the interaction of poly-L-lysine with dipalmitoylphosphatidylglycerol bilayers, *Biophys. J.* (1984) [https://doi.org/10.1016/S0006-3495\(84\)84047-3](https://doi.org/10.1016/S0006-3495(84)84047-3).
- [54] B.F. Bell, M. Schuler, S. Tosatti, M. Textor, Z. Schwartz, B.D. Boyan, Osteoblast response to titanium surfaces functionalized with extracellular matrix peptide biomimetics, *Clin. Oral Implants Res.* (2011) <https://doi.org/10.1111/j.1600-0501.2010.02074.x>.
- [55] E. Varoni, E. Canciani, B. Palazzo, V. Varasano, P. Chevallier, L. Petrizzi, C. Dellavia, D. Mantovani, L. Rimondini, Effect of poly-L-lysine coating on titanium osseointegration: from characterization to in vivo studies, *J. Oral Implantol.* (2015) <https://doi.org/10.1563/aaid-joi-d-13-00036>.
- [56] E. Takai, K.D. Costa, A. Shaheen, C.T. Hung, X.E. Guo, Osteoblast elastic modulus measured by atomic force microscopy is substrate dependent, *Ann. Biomed. Eng.* (2005) <https://doi.org/10.1007/s10439-005-3555-3>.
- [57] A. Krause, E.A. Cowles, G. Gronowicz, Integrin-mediated signaling in osteoblasts on titanium implant materials, *J. Biomed. Mater. Res.* (2000) [https://doi.org/10.1002/1097-4636\(20001215\)52:4<738::AID-JBM19>3.0.CO;2-F](https://doi.org/10.1002/1097-4636(20001215)52:4<738::AID-JBM19>3.0.CO;2-F).
- [58] P. Tryoen-Th, D. Vautier, Y. Haikel, J.C. Voegel, P. Schaaf, J. Chluba, J. Ogier, Viability, adhesion, and bone phenotype of osteoblast-like cells on polyelectrolyte multilayer films, *J. Biomed. Mater. Res.* (2002) <https://doi.org/10.1002/jbm.10110>.
- [59] T. Wang, X. Yang, X. Qi, C. Jiang, Osteoinduction and proliferation of bone-marrow stromal cells in three-dimensional poly (ϵ -caprolactone)/hydroxyapatite/collagen scaffolds, *J. Transl. Med.* (2015) <https://doi.org/10.1186/s12967-015-0499-8>.
- [60] C.R. Wittmer, J.A. Phelps, W.M. Saltzman, P.R. Van Tassel, Fibronectin terminated multilayer films: protein adsorption and cell attachment studies, *Biomaterials.* (2007) <https://doi.org/10.1016/j.biomaterials.2006.09.037>.
- [61] M.S. Liberio, M.C. Sadowski, C. Soekmadji, R.A. Davis, C.C. Nelson, Differential effects of tissue culture coating substrates on prostate cancer cell adherence, morphology and behavior, *PLoS One.* (2014) <https://doi.org/10.1371/journal.pone.0112122>.
- [62] J.S. Heo, H.O. Kim, S.Y. Song, D.H. Lew, Y. Choi, S. Kim, Poly-L-lysine prevents senescence and augments growth in culturing mesenchymal stem cells ex vivo, *Biomed Res. Int.* (2016) <https://doi.org/10.1155/2016/8196078>.
- [63] L. Cai, J. Lu, V. Sheen, S. Wang, Optimal poly(L-lysine) grafting density in hydrogels for promoting neural progenitor cell functions, *Biomacromolecules.* (2012) <https://doi.org/10.1021/bm300381d>.
- [64] H. Lu, L. Guo, N. Kawazoe, T. Tateishi, G. Chen, Effects of poly(L-lysine), poly(acrylic acid) and poly(ethylene glycol) on the adhesion, proliferation and chondrogenic differentiation of human mesenchymal stem cells, *J. Biomater. Sci. Polym. Ed.* (2009) <https://doi.org/10.1163/156856209X426402>.
- [65] D. Galli, L. Benedetti, M. Bongio, V. Maliardi, G. Silvani, G. Ceccarelli, F. Ronzoni, S. Conte, F. Benazzo, A. Graziano, G. Papaccio, M. Sampaolesi, M.G. Cusella De Angelis, In vitro osteoblastic differentiation of human mesenchymal stem cells and human dental pulp stem cells on poly-L-lysine-treated titanium-6-aluminium-4-vanadium, *J. Biomed. Mater. Res. - Part A* (2011) <https://doi.org/10.1002/jbm.a.32996>.
- [66] A. Mitchell, L. Ashton, X.B.B. Yang, R. Goodacre, A. Smith, J. Kirkham, Detection of early stage changes associated with adipogenesis using Raman spectroscopy under aseptic conditions, *Cytom. Part A.* 87A (2015) 1012–1019, <https://doi.org/10.1002/cyto.a.22777>.
- [67] W. Qi, W. Yuan, J. Yan, H. Wang, Growth and accelerated differentiation of mesenchymal stem cells on graphene oxide/poly-L-lysine composite films, *J. Mater. Chem. B* 2 (2014) 5461–5467, <https://doi.org/10.1039/C4TB00856A>.
- [68] A.M. Buo, M.S. Williams, J.P. Kerr, J.P. Stains, A cost-effective method to enhance adenoviral transduction of primary murine osteoblasts and bone marrow stromal cells, *Bone Res.* (2016) <https://doi.org/10.1038/boneres.2016.21>.
- [69] H. Follet, G. Boivin, C. Rumelhart, P.J. Meunier, The degree of mineralization is a determinant of bone strength: a study on human calcanei, *Bone.* (2004) <https://doi.org/10.1016/j.bone.2003.12.012>.
- [70] G. Boivin, D. Farlay, Y. Bala, A. Doublier, P.J. Meunier, P.D. Delmas, Influence of remodeling on the mineralization of bone tissue, *Osteoporos. Int.* (2009) <https://doi.org/10.1007/s00198-009-0861-x>.
- [71] A.J. Hobro, N.I. Smith, An evaluation of fixation methods: spatial and compositional cellular changes observed by Raman imaging, *Vib. Spectrosc.* (2017) <https://doi.org/10.1016/j.vibspec.2016.10.012>.
- [72] F. Draux, C. Gobinet, J. Sulé-Suso, A. Trussardi, M. Manfait, P. Jeannesson, G.D. Sockalingum, Raman spectral imaging of single cancer cells: probing the impact of sample fixation methods, *Anal. Bioanal. Chem.* (2010) <https://doi.org/10.1007/s00216-010-3759-8>.
- [73] M.A.B. Hedegaard, K.L. Cloyd, C.M. Horejs, M.M. Stevens, Model based variable selection as a tool to highlight biological differences in Raman spectra of cells, *Analyst.* (2014) <https://doi.org/10.1039/c4an00731j>.
- [74] A.D. Meade, C. Clarke, F. Draux, G.D. Sockalingum, M. Manfait, F.M. Lyng, H.J. Byrne, Studies of chemical fixation effects in human cell lines using Raman microspectroscopy, *Anal. Bioanal. Chem.* (2010) <https://doi.org/10.1007/s00216-009-3411-7>.
- [75] L.L. McManus, F. Bonnier, G.A. Burke, B.J. Meenan, A.R. Boyd, H.J. Byrne, Assessment of an osteoblast-like cell line as a model for human primary osteoblasts using Raman spectroscopy, *Analyst.* (2012) <https://doi.org/10.1039/c2an16209a>.
- [76] G.S. Mandair, P. Steenhuis, M.A. Ignelzi, M.D. Morris, Bone quality assessment of osteogenic cell cultures by Raman microscopy, *J. Raman Spectrosc.* (2019) <https://doi.org/10.1002/jrs.5521>.
- [77] C. Kallepitis, M.S. Bergholt, M.M. Mazo, V. Leonardo, S.C. Skaalure, S.A. Maynard, M.M. Stevens, Quantitative volumetric Raman imaging of three dimensional cell cultures, *Nat. Commun.* (2017) <https://doi.org/10.1038/ncomms14843>.
- [78] A.R. Boyd, G.A. Burke, B.J. Meenan, Monitoring cellular behaviour using Raman spectroscopy for tissue engineering and regenerative medicine applications, *J. Mater. Sci. Mater. Med.* (2010) <https://doi.org/10.1007/s10856-009-3965-0>.
- [79] P. Vandenabeele, *Practical Raman Spectroscopy: An Introduction*, Wiley & Sons, Chichester, UK, 2013.
- [80] J. Trevisan, P.P. Angelov, A.D. Scott, P.L. Carmichael, F.L. Martin, IRootLab: a free and open-source MATLAB toolbox for vibrational biospectroscopy data analysis, *Bioinformatics.* (2013) <https://doi.org/10.1093/bioinformatics/btt084>.

-
- [81] K.A. Staines, B. Javaheri, P. Hohenstein, R. Fleming, E. Ikegbu, E. Unger, M. Hopkinson, D.J. Buttle, A.A. Pitsillides, C. Farquharson, Hypomorphic conditional deletion of E11/podoplanin reveals a role in osteocyte dendrite elongation, *J. Cell. Physiol.* (2017) <https://doi.org/10.1002/jcp.25999>.
- [82] E. Ikegbu, L. Basta, D.N. Clements, R. Fleming, T.L. Vincent, D.J. Buttle, A.A. Pitsillides, K.A. Staines, C. Farquharson, FGF-2 promotes osteocyte differentiation through increased E11/podoplanin expression, *J. Cell. Physiol.* 233 (2018) 5334–5347, <https://doi.org/10.1002/jcp.26345>.
- [83] X. Yang, J.T. Hatfield, S.J. Hinze, X. Mu, P.J. Anderson, B.C. Powell, Bone to pick: the importance of evaluating reference genes for RT-qPCR quantification of gene expression in craniosynostosis and bone-related tissues and cells, *BMC Res. Notes.* (2012) <https://doi.org/10.1186/1756-0500-5-222>.
- [84] K.J. Livak, T.D. Schmittgen, Analysis of relative gene expression data using real-time quantitative PCR and the $2^{-\Delta\Delta CT}$ method, *Methods.* 25 (2001) 402–408, <https://doi.org/10.1006/meth.2001.1262>.